POLITECNICO DI TORINO
Repository ISTITUZIONALE

UV telescope TUS on board Lomonosov satellite: Selected results of the mission

(Article begins on next page)

20 April 2024

UV telescope TUS onboard Lomonosov satellite: selected results of the mission

Dario Barghini[a,b], Mario Bertaina[a,*], Alberto Cellino[b], Francesco Fenu[a,b], Silvia Ferrarese[a], Alessio Golzio[a], Oliver I. Ruiz-Hernandez[c], Pavel Klimov[d], Antonio Montanaro[a,1], Anthony Salsi[a,2], Sergei Sharakin[d], Ksenia Sigaeva[d,e], Mikhail Zotov[d]

[a]Department of Physics - University of Turin, Via P. Giuria 1, Turin 10126, Italy
[b]National Institute of Astrophysics - Astrophysical Observatory of Turin, Via Osservatorio 20, Pino Torinese 10025, Italy
[c]Benemérita Universidad Autónoma de Puebla, Facultad de Ciencias Físico Matemáticas,
Avenida San Claudio y 18 Sur, C.P. 72570, Puebla, México
[d]Skobeltsyn Institute of Nuclear Physics - Lomonosov Moscow State University, 1(2), Leninskie gory, Moscow 119991, Russia
[e]Faculty of Physics - Lomonosov Moscow State University, 1(2), Leninskie gory, Moscow 119991, Russia

Abstract

The Tracking Ultraviolet Setup (TUS) was the first orbital detector aimed to check the possibility of recording ultra-high energy cosmic rays (UHECRs) at $E \gtrsim 100$ EeV by measuring the fluorescence signal of extensive air showers in the atmosphere. TUS was an experiment funded by the Russian Space Agency ROSCOSMOS, and it operated as a part of the scientific payload of the Lomonosov satellite since April 2016 till late 2017. During its mission, TUS registered almost 80,000 events in its main operation mode, with a few of them being sufficiently interesting to be more deeply scrutinized as they showed light profile and duration similar to UHECR events, even though much brighter. At the same time, the data acquired by TUS in different acquisition modes have been used to search for more exotic matter such us strangelets and nuclearites, and to measure occurrence, time profile and signal amplitude of different classes of transient luminous events among other scientific objectives, showing the interdisciplinary capability of a space-based observatory for UHECRs. In this paper, we report a selection of studies and results obtained with the TUS telescope which will be presented and placed in the contest of the present and future missions dedicated to the observation of UHECRs from space such as Mini-EUSO, K-EUSO and POEMMA.

1. Introduction

The cosmic ray spectrum spans over 11 orders of magnitude in energy and reaches limits well beyond those of the most powerful accelerators created by mankind. Above 10^{18} eV, these particles are called ultra-high energy cosmic rays (UHECRs).

At energies above 5×10^{19} eV, UHECR sources probably involve physical processes occurring in extreme extragalactic environments as very few known astrophysical objects can satisfy the requirements imposed by the observed spectrum, composition, and lack of strong anisotropies (Kotera & Olinto, 2011). At this energy, the flux becomes as low as one event per century per square kilometer (Aab et al., 2020). Therefore, huge areas are necessary to collect enough statistics.

A space-based detector devoted to UHECR science has the advantage of a very large exposure and a uniform coverage of the celestial sphere. The idea of space-based observation of UHECRs was first proposed in the late 70s, in response to

---
*Corresponding author: Tel.: +39-011-670-7492; fax: +39-011-670-7497;
Email address: bertaina@to.infn.it (Mario Bertaina)
[1]Now at: DET Department of Electronics and Telecommunications - Politecnico di Torino, Corso Duca degli Abruzzi, 24, Turin 10129, Italy
[2]Now at: Laboratoire Lagrange - Observatoire de la Côte D'Azur, Boulevard de l'Observatoire, CS 34229, Nice 06304, France

a NASA Call for Projects and Ideas in High Energy Astrophysics for the 1980s with the Satellite Observatory of Cosmic Ray Showers (SOCRAS) concept (Benson & Linsley, 1981). Along the years several concepts were elaborated like OWL in the United States (Stecker et al., 2004) and EUSO in Europe (Parmar et al., 2013), which later on evolved into the JEM-EUSO mission (Adams Jr. et al., 2015c). In Russia, the space program KOSMOTEPETL, which included the KLYPVE and TUS projects, was announced in 2001 (Khrenov et al., 2001). In 2016, TUS was successfully launched as a payload of the Lomonosov satellite and operated in space between April 2016 and late 2017 (Khrenov et al., 2017; Klimov et al., 2017). In parallel, in 2013, when it became clear that the JEM-EUSO mission could not be realized, the JEM-EUSO collaboration re-oriented the efforts into a rich program of missions from ground (EUSO-TA (Abdellaoui et al., 2018)), stratospheric balloons (EUSO-Balloon (Adams Jr. et al., 2015a), EUSO-SPB1 (Wiencke & Olinto, 2017), and EUSO-SPB2 (Adams Jr. et al., 2017)), and in space under the name "Joint Experiment Missions: Extreme Universe Space Observatory" (Bertaina, 2021). Concerning the space missions, the Mini-EUSO detector was developed and launched in August 2019 on the International Space Station (Bacholle et al., 2021). The KLYPVE and JEM-EUSO collaborations joined the efforts to develop the KLYPVE-EUSO (K-EUSO in short), mission (Casolino et al., 2017). At this stage, TUS was included as an adjunct project of the program for its relevance to the development of K-EUSO and in general to the future missions of the program, such as POEMMA (Olinto et al., 2021).

The principle of observation of all the so far conceived space-based missions relies on the detection of UV light emitted by isotropic fluorescence of atmospheric nitrogen excited by the extensive air showers (EASs) in the Earth's atmosphere and of forward-beamed Cherenkov radiation reflected from the Earth's surface or from dense cloud tops. The design of a space-based telescope for UHECR observation has strong constraints on power, mass, size and data transmission bandwidth and requires the development of a number of novel technologies, from optics to sensors, front-end and read-out electronics. The various experiments and pathfinder missions, such as TUS, are essential in pursuing this effort. In this regards, the studies and results obtained with the TUS telescope are important also in the contest of the present and future missions devoted to the observation of UHECRs from space (Mini-EUSO, K-EUSO or POEMMA) as they allow developing methodologies that can be applied elsewhere. Moreover, TUS demonstrated that a space detector with the primary goal of searching for extremely energetic particles, is in reality a multi-disciplinary instrument with an extremely wide science reach and with unique sensitivity for those phenomena.

This work reports on selected results of the TUS mission, beginning from the UHECR science but providing also examples of its multi-disciplinary capabilities. The paper is structured in the following way. Section 2 summarizes the key elements of the detector. Section 3 reports on the efforts which have been done to implement the TUS configuration into the simulation software adopted for the interpretation of the data. A methodological study to estimate TUS exposure to UHECR is treated in Section 4. The importance of an accompanying atmospheric study to interpret the data and the tools used for this purpose are described in Section 5. The result of the search for UHECRs in the data collected by TUS is discussed in Section 6. Section 7 provides examples of anomalous events detected in the UHECR trigger mode, which have an atmospheric discharge origin. The paper continues with the description of the search for much slower light tracks such as due to meteors (Section 8) or hypothetical exotic forms of matters such as nuclearites (Section 9), and ends with slow phenomena which have a much wider spatial extension such as auroral lights (Section 10). Conclusions and perspectives are outlined in Section 11.

2. The TUS detector on board the Lomonosov satellite

The TUS detector is the first attempt to measure UHECR fluorescent light from space. It was launched on April 28, 2016, on a polar sun-synchronous orbit with inclination of 97.3°, period of ~94 min, and altitude about 500 km. TUS was operated regularly till late November 2017, when the Lomonosov satellite faced some technical problems that did not allow transmitting experimental data to Earth.

The TUS detector consisted of two main parts: a parabolic mirror-concentrator of the Fresnel type and a square-shaped 256-pixel photodetector in the focal plane of the mirror (see Fig. 1). The mirror had an area of about 2 m^2 with a focal distance of 1.5 m. A pixel field of view equals 10 mrad, which results in spatial resolution of 5 km, and the overall TUS field of view (FoV) is approximately 80 km $\times$ 80 km at the sea level. Each pixel of the TUS photodetector is a Hamamatsu R1463 photomultiplier tube. Light guides with square entrance apertures (15 mm $\times$ 15 mm) and circular outputs were employed to fill uniformly the detector's FoV. Each pixel has a black blind 1 cm above the light guide to protect it from stray light. An UV filter of 13 mm diameter and 2.5 mm thickness is placed in front of each PMT. The pixels are grouped in 16 identical photodetector modules. Each cluster has its own digital data processing system for the first-level trigger, based on a Xilinx Field-Programmable Gate Array (FPGA), and a high voltage power supply, controlled by the FPGA. The central processor board gathers information from all modules, controls their operation, and implements the second-level trigger algorithm, see (Klimov et al., 2017; Khrenov et al., 2017) for details.

The TUS electronics could operate in four modes intended for detecting various fast optical phenomena in the atmosphere at different time scales with different time sampling. The main mode was aimed at registering UHECRs and had a time sampling of 0.8 μs. This mode was also efficient for short transient luminous events (TLEs) measurements, for example, ELVEs ("ELVE" stands for Emission of Light and Very low frequency perturbation from an Electromagnetic pulse). Slower modes had time sampling of 25.6 μs, 0.4 ms (for studying TLEs of different kinds slower than ELVEs: sprites, blue jets, gigantic jets, etc.). An even slower mode of 6.6 ms was dedicated to the detection of micro-meteors and thunderstorm activity at a longer time scale. The four operational modes could not be run
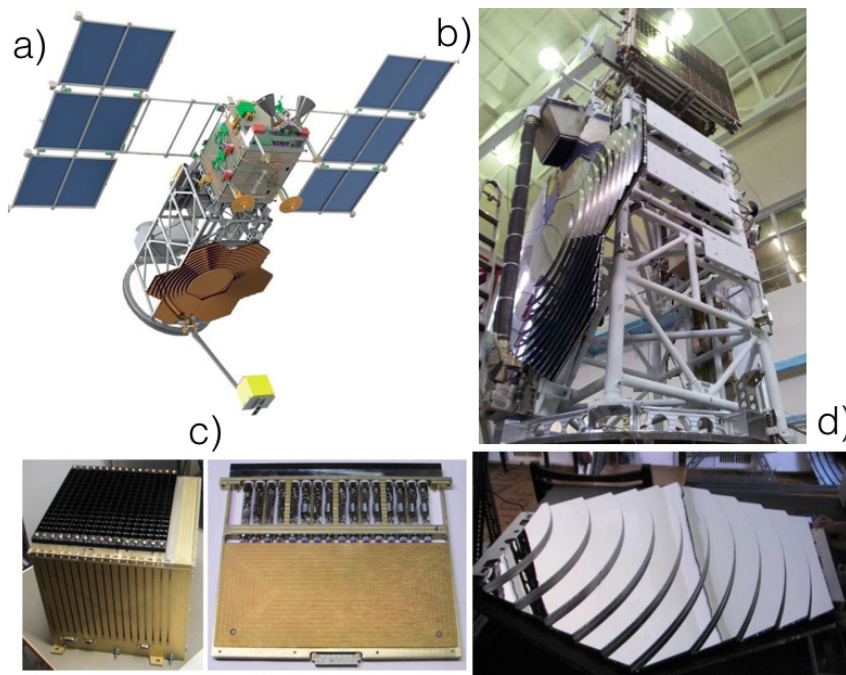
Fig. 1. a) Artist's view of the TUS detector on board the Lomonosov satellite; b) TUS on board the Lomonosov satellite during preflight preparations at cosmodrome Vostochny; c) TUS focal surface; d) a segment of the TUS Fresnel mirror.

in parallel, therefore, the selected mode had to be fixed at the start of a run. Waveforms in each mode consisted of 256 time samples.

The trigger scheme, common to all four modes was structured in two steps to allow background rejection and the acceptance of the cosmic ray events. A fast ADC converted analogue signals of PMTs into digital codes with the resolution of $0.8\,\mu$s. The digitized signals are summed up on a sliding window of 16 frames for each photomultiplier. The integrated values are compared then with a preset threshold on a moving matrix of 3×3 contiguous pixels. The first level trigger is activated in case the threshold is overcome for any of such pixels. The persistence of such a signal excess is then tested each 16 frames. Once the persistence is longer than a predetermined value, the second level trigger is issued and the data transfer is initiated. The Block of Information unit, which managed the data acquisition for all scientific devices on board the Lomonosov satellite, could accept data from TUS at most once in 53–60 seconds. This external constraint imposed a lower limit to the acquisition dead time of the TUS detector. This limitation had a severe impact on part of the analyses that are discussed in the following. Namely, ground flasher lights could not be triggered more than once and clearly recognized as repetitive signals; the estimation of the exposure had to assume that the detector was always operational among triggers; during the 50–60 seconds of dead time, the detector shifted the position by ~400 km. Therefore, when the

trigger capability is restored, the FoV has totally changed and might not be representative anymore of the monitored conditions at the time of the last trigger. During an accident at the beginning of the mission, 20% of the PMTs were destroyed and sensitivities of the remaining PMTs changed in comparison with pre-flight measurements. A number of attempts of in-flight calibration have been performed but none of them is fully reliable yet. This introduces a large factor of uncertainty in estimates of the trigger threshold and the signal intensity. Due to this all respective estimates presented below are approximate.

3. ESAF Simulation

During its operation, TUS detected about $8 \cdot 10^4$ events in the main mode of operation, which have been subject to an offline analysis to select among them those satisfying basic temporal and spatial criteria of UHECRs. A few events passed this first screening. In order to perform a deeper analysis of such candidates, a dedicated version of ESAF (EUSO Simulation and Analysis Framework), (Berat et al., 2010) which includes a modeling of TUS optics and detector responses, has been developed. ESAF takes care of the simulation of all the relevant processes from the shower simulation until the event reconstruction. Several shower simulators are implemented in ESAF, following parametric and Monte Carlo approaches, such as SLANT-GIL (Ilina et al., 1992), CORSIKA (Heck et al.,

1990), and CONEX (Pierog et al., 2004). Both fluorescence and Cherenkov light (reflected and back-scattered) productions are taken into account in ESAF. The fluorescence spectrum is simulated according to (Nagano et al., 2004). The Cherenkov reflection is treated according to a Lambertian reflector. Therefore, all the photons are reflected diffusely due to the very irregular terrestrial surface with an albedo which is surface dependent: 5% for water and forests, 2% for savannah, 85% on fresh snow, to provide a few examples. All the photons are affected by Rayleigh scattering and ozone absorption. Optionally, clouds can be simulated as a constant layer of variable altitude thickness and optical depth. Non-uniform cloud coverage is also included in ESAF. Once the photons reach the detector, they are taken over by the optics module and later on the Focal Surface (FS) response is simulated.

In the past years, the ESAF software has been upgraded to simulate the response of the JEM-EUSO instrument (Fenu et al., 2021) and of other telescopes of the program, including the TUS detector directly into the ESAF simulation code (instead of the previously used approach, where ESAF was used to generate the EAS cascade and the fluorescent radiation, and the additional software TUSSIM (Tkachev et al., 2015) was used to simulate the TUS detector performance).

Regarding the optics, two approaches have been developed in parallel. The first one adopts a parametric simulation module that calculates analytically the position of a photon on the focal surface and adds a Gaussian spread around this position. This is intended to be a fast working tool to test the features of the different optics designs in an approximated way. It is used in the exposure study, where several thousands of EASs are simulated. Second, a full ray-trace code is used in the actual optics design. As an example, this is used in the nuclearite study. Once the photons reach the FS, they are transported through the filter and the optical adapter before reaching the photocathode. All the relevant effects including geometrical losses, inefficiencies of the adapter and of filters are taken into account. A parametrization of the photomultiplier response is included in the electronics part. Quantum efficiency, dependence on the incident angle of photon, collection efficiency and cross talk are also taken into account. The signal is then amplified by a parameterized gain and the resulting output current is collected and treated by the Front End Electronics module. Fig. 2 shows an example of the light profile and shower track expected to be detected from a 10^{21} eV EAS with 60° zenith angle proton EAS.

ESAF was extensively used to provide the first estimation of the geometrical exposure of the mission for UHECR observation as well as to deeply scrutinize a few detected events. Results of these studies are reported in Sections 4 and 6.

4. Exposure study

The estimation of the geometrical exposure for space-based observatories is a much more complex topic than from ground-based ones, as the atmospheric and illumination conditions are rapidly changing due to the satellite speed. The study reported in the following is based on events triggered in the EAS mode

in the night segments of the Lomonosov orbits. For each trigger, 256 time frames with the signal of all pixels together with other information such as the satellite position and speed vector are available. Data have been acquired in several discontinuous sessions, with the highest exposure gathered in Autumn 2016 and in the second half of 2017. The interruptions were mainly related to the operation in other acquisition modes. Figure 3 shows the geographical distribution of the triggers.

The triggers are distributed quite uniformly with a higher concentration over continents. A notable exception to this is represented by Antarctica, the Arctic and Sahara, which remain quiet areas with the trigger densities comparable to those above the oceans.

As we have already mentioned above, TUS had a dead time of 53–60 seconds after each trigger, the exact value depending on the mission period. The time that the satellite used to take to cross the night side of the Earth was ~ 2000 seconds. Thus, no orbits with more than ~ 40 triggers could be generally observed. An estimate of the active time can be therefore given for each orbit, under the assumption that the detector has always been in acquisition, except for the intrinsic dead time. 3118 orbits with a total acquisition time of 73 full days are identified. A total active time of 31 days is obtained as soon as the dead time is taken into account. This amounts to ~42% of the total acquisition time. Such an estimate is based only on the identified orbits and could be potentially an underestimate of the real acquisition time. Thanks to the knowledge of the satellite trajectory, it was possible to estimate with a ~1 second resolution the status of the detector for each position on the Earth map. Fig. 4 shows the active time fraction of the satellite as a function of the geographical coordinate.

It can be clearly seen that the presence of a higher trigger rate implies a higher dead time. As a consequence of that, populated areas or stormy regions are basically not contributing to the cumulative exposure. Aurora ovals are also clearly visible as non-active areas in the polar regions. On the other hand, oceans are very quiet areas, where UHECR studies would be favoured. Positions of the Sun and the Moon were calculated based on data from the Japanese Coast Guard (2021). The presence of low or no-Moon illumination is verified in 21.2 full days of acquisition. The amount of active time in this condition amounts to 12.9 days, 60% of moonless acquisition time. The cloud condition for each trigger has been estimated based on (MERRA data, 2021).

Fig. 5 shows the fraction of events where the cloud top height h is lower than a threshold h_{thr}. It can be seen how most ($\sim 70\%$) of the triggers are in cloudy conditions. It is therefore crucial to estimate the efficiency for UHECR detection in presence of clouds. ESAF simulations are used for this, following the approach described in (Adams Jr. et al., 2013).

The signal recorded for each triggered event can be used to estimate the rate of photoelectrons generated by the airglow emission. Such information is used in the simulations to estimate the energy dependence of the exposure. In general, the rate of the background illumination varies from 1 to over 100 photoelectrons per frame unless rare cases such as above auroral ovals, night-day transitions, very populated areas, which
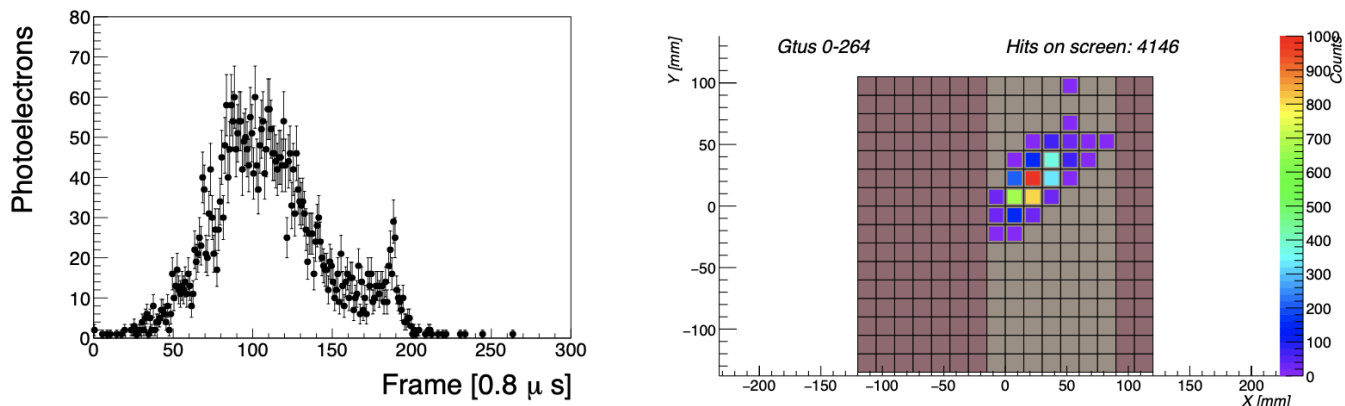
Fig. 2. A 10^{21} eV, 60° zenith angle proton event. On the left: the photoelectron profile for the TUS detector; the bump around frame 190 is due to the Cherenkov reflection when the EAS reaches the ground. On the right: the photoelectron image for TUS.
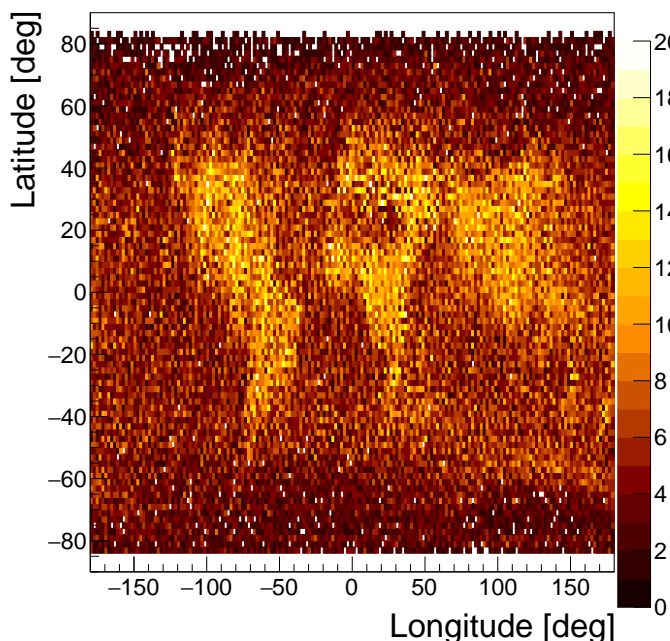

Fig. 3. Geographical distribution of the triggers in the EAS mode. The color scale indicates the number of triggers in each bin.
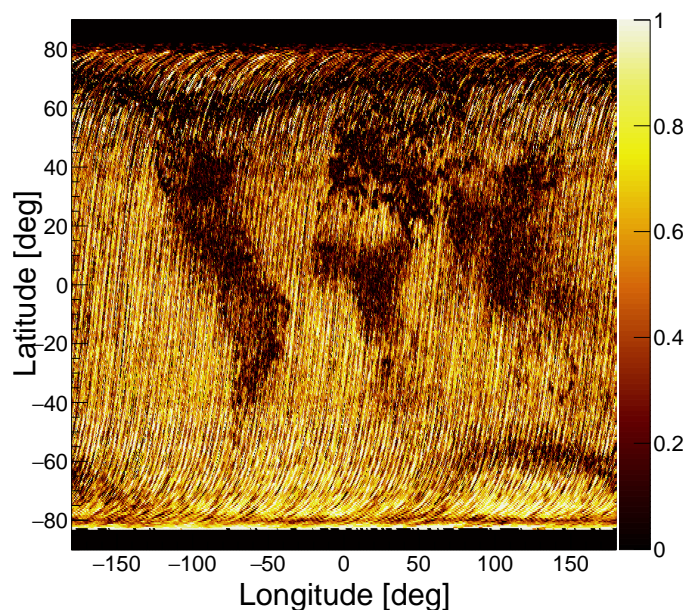

Fig. 4. Ratio of active time over the total amount of transit time as a function of geographical location.

anyway do not contribute significantly to the exposure as previously discussed.

The trigger performance is derived through Monte Carlo simulations. Two thousand EASs were injected in an area A_{simu} larger than the field of view (±150 km) to avoid border effects. Showers were simulated with zenith angles θ from 0° to 90° with a $\sin(2\theta)$ dependence and the azimuth from 0° to 360° uniformly. The TUS trigger logic was implemented in the ESAF simulation software and used for this estimation. Several trigger thresholds adopted in the mission were tested with an airglow rate of ~18 photoelectrons per frame. The estimate of the trigger performance depends on a number of factors, among them the sensitivity of the photodetector, the level of the background illumination and software parameters of the trigger. As

a result of taking into account the currently most accurate estimates based on the in-flight calibration that will be reported in detail elsewhere, we obtain a trigger threshold $\gtrsim$ 500 EeV. Moreover, the majority of the events could indeed trigger only above $\theta \approx$ 40°–50°. This is a consequence of the persistence condition of the trigger that rejects all events lasting for a short time, therefore, the most vertical ones.

Secondly, the efficiency of the trigger in cloudy conditions is simulated. One thousand EASs at fixed energy have been simulated for each cloud top height condition in similar way as for clear sky. Table 1 presents the fraction of triggers with clouds below a specific height (as shown in Fig. 5 and indicated as $\eta(h < h_{thr})$). The second row of Table 1 shows the ratio of the efficiency obtained in cloudy conditions ϵ_{cloud} to the one obtained in clear sky (ϵ_{cs}).
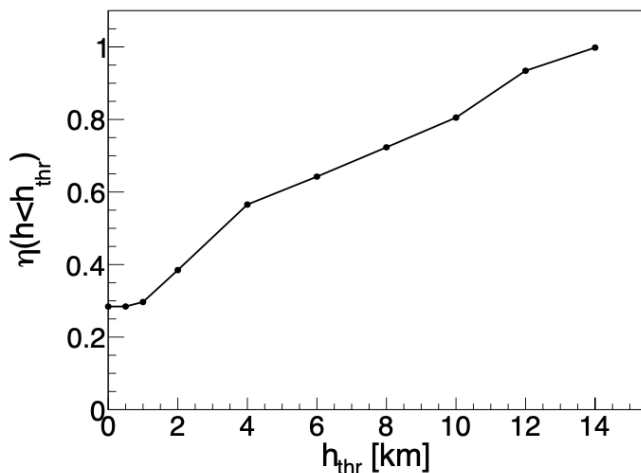
Fig. 5. Fraction of triggers with cloud top height below h_{thr} (see the text for details).

Table 1. Reduction of the trigger efficiency due to the presence of clouds with respect to clear sky at $2 \cdot 10^{21}$ eV.

	Clear sky	h_{thr}=2 km	6 km	10 km	14 km
$\eta(h < h_{thr})$	28%	38%	64%	80%	99.8%
$\epsilon_{cloud}/\epsilon_{cs}$	100%	83%	40%	6%	0%

A higher cloud top height causes a significant reduction of the triggered events given the reduction of the amount of light reaching the detector. An estimate of the overall reduction of the exposure in the whole flight can be given by an average of the trigger efficiency weighted by the fraction of triggers in each condition. This leads to 57% of what is expected for the clear sky case. By taking into account the above factors, excluding the cloud impact, the geometrical exposure in clear sky conditions amounts to ~1550 km^2 sr yr. This value reduces to ~884 km^2 sr yr at $2 \cdot 10^{21}$ eV as soon as the cloud impact is taken into account. We remind that the estimation of the exposure might have a cloud dependence due to the interplay of the brightness of the shower and the location of its maximum. At lower energies, a lower value for the exposure is expected. A more detailed study of the exposure will be reported in a dedicated publication.

5. Weather studies

The previous section dealt with the attenuation of the signal related to the cloud cover (see Table 1), so it is crucial to know the atmospheric conditions, such as the cloud coverage or lightning activity below the telescope, to avoid the misinterpretation of a light signal with something that is related to tropospheric phenomena, or to estimate the quality of the observation capabilities. When long-term cosmic ray measurements are conducted from space (such as the TUS observations), the observed Earth' surface can be covered by clouds, position and thickness of which can continuously change, therefore the knowledge of the time evolution of weather conditions is necessary.

Several tools are at disposal of meteorologists to determine the weather in a particular area of the world. They can be classified in two main categories: weather observations and weather models (in analysis mode, so studying the past). Among the weather observations, the weather maps and the satellite observations are useful to localize the cloud positions and its thickness.

In order to individuate the cloud coverage and the cloud type (altitude of the base and the top of the cloud) that allow one to know which atmospheric processes are expected or if clear atmospheric conditions are present, the first step is always to analyse the weather maps, where the ground observations match with the main pressure gradients (fronts) and the active weather areas are depicted. As a second step, it is extremely useful to consider satellite images in infrared bands since an UHECR is to be measured during nighttime. At the same time, it is very valuable to look at composite images obtained by mixing different bands. Those images are then enhanced with the primary colors (d'Entremont & Thomason, 1987). In this way, the main cloud structures are identified, and considering different bands, colors and sensitivity of the satellite, it is possible to estimate the cloud top altitude from its temperature and shape. Other satellite products, results of the elaboration of satellite images through complex algorithms, permit to directly have the cloud mask (see Figs. 12 and 14 below) or the cloud layers as output. Higher-quality analysis is obtained by combining weather maps (with fronts and isobars), obtained by ground observations, with satellite images. To complete the analysis, the lightning activity through ground based detectors of the National Lightning Detection Network (USA) can also be considered.

In the present paper, the weather conditions have been derived by the observations available from satellites (e.g., a re-analysis of MERRA-2 data set), soundings, weather stations and weather charts to study the exposure to cosmic rays (Section 4) and nuclearites (Section 9).

The second category of tools, the weather models, in particular the Global Circulation Models (GCM), are extremely useful to determine the weather conditions everywhere and at any time in the Earth's troposphere. Through the data assimilation procedures (Rodell et al., 2004; Bonavita et al., 2015), the GCM considers and interpolates all the available and previously described observations. The GCM outputs are used in the analysis of the TUS event detected over Sardinia and described in Section 7, and a first guess on the weather situation is provided. Figure 6 shows the medium cloud cover as computed by the GCM of the Global Forecasting System close in time to the Sardinia event TUS0905, see below. Usually, this parameter is the most useful to detect towering clouds as cumulonimbus that are associated with lightnings.

Sometimes an in-depth analysis is required for an event detected at a defined time and location. In this case, the application of regional models (initialised with GCM boundary conditions) could significantly enhance the spatial, vertical and time resolution of the weather conditions description. The application of some algorithms that compute the cloud-base or cloud-top altitude (Anzalone et al., 2019) help in the finer description of the cloud structures.
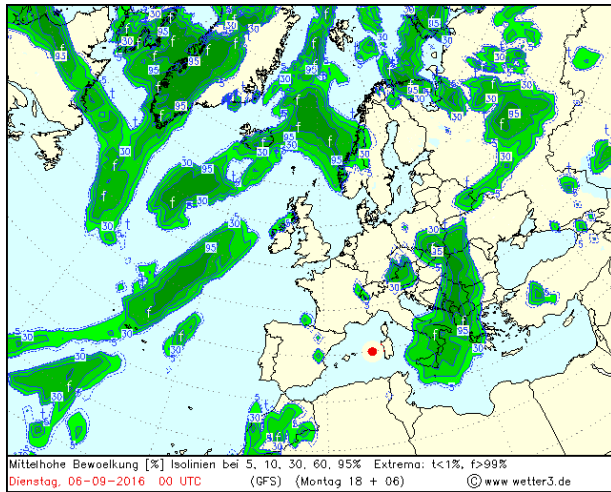
Fig. 6. Global Forecasting System analysis at 0000 UTC on September 6, 2016, roughly one hour later the TUS detected an event. The medium cloud cover is represented with green areas. The red dot shows the position of the TUS event.

6. EAS-like events

An algorithm to search for signals arising from extensive air showers (EASs) initiated by UHECRs was developed on the basis of intensive simulations with ESAF (Berat et al., 2010). Thousands of EAS were simulated in the energy range from 100 EeV to 1100 EeV arriving at different zenith angles and crossing the FoV at different positions. The response of the detector was calculated for a range of PMT gains from 10^5 to $2 \cdot 10^6$ for a wide range of intensities of the background illumination. With these data at hands, we performed an analysis of the quality of fitting of individual waveforms with several asymmetric parametric functions (including the bi-Gaussian and skew Gaussian functions), which demonstrated a high quality of fitting in terms of the coefficient of determination R^2 together with a high robustness of the procedure. We obtained a range of possible values of fitting parameters as found for the simulated signals and applied them to the experimental data as a pattern recognition criteria. The procedure lead to selecting almost 120 TUS events the waveforms of which satisfied the conditions. We shall call them EAS-like events in what follows.

These events have a characteristic light curve (integral signal of all triggered channels) with a pronounced maximum and full duration at half-maximum (FDHM) from 40 to 80 μs, which is quite consistent with the simulated detector response to the EAS fluorescence (see Fig. 2). However, the amplitude of all EAS-like events corresponds to UHECR energies well above 10^{20} eV, and, consequently, their number is two orders of magnitude higher than can be expected taking into account the limited exposure of the TUS experiment. Moreover, the majority of EAS-like events were registered above continents with half of them above the USA, which immediately raises the question of their possible anthropogenic origin.

Another feature of a simulated non-vertical EAS event is the presence of a noticeable movement of the signal along the photodetector matrix: the hit pixels are lined up along a rectilinear "track", and the displacement velocity is approximately pro-

portional to $\tan(\theta/2)$, where θ is the zenith angle of the arrival direction. The aberrations of the TUS mirror lead to smearing of this track over neighboring pixels, which significantly complicates the determination of motion. It turned out that only in 6 events the track length was sufficient to identify the movement of the image, reconstruct the track, and estimate the direction of arrival.

Probably the most interesting of the EAS-like events is the TUS161003 event registered above Minnesota, USA, see a detailed discussion in (Khrenov et al., 2020). The event demonstrates waveforms and light curve with form and kinematics similar to those expected from an EAS but the amplitude corresponds to UHECR energies $\gtrsim 10^{21}$ eV, which makes the cosmic ray origin of this event highly unlikely. It was found that a similar signal (with FDHM $\sim 50\,\mu$s) can be produced by a pair of flashers with a specific choice of parameters. A possibly more interesting interpretation of the TUS161003 event is a shower initiated by a relativistic dust grain (Khrenov et al., 2021). The latter opportunity is currently under analysis.

Five other EAS-like events demonstrated a similar behaviour. They were also registered above the USA but airports were found in their close vicinity. A dedicated analysis showed that reconstructed arrival directions of all these events strongly correlate with directions of airport runways (Sharakin & Ruiz Hernandez, 2021), see Fig. 7 where a reconstructed (magenta) track of TUS161031a and (yellow) runway of the Sparrevohn AFC Airport are presented inside the FoV of 8 hit pixels. This witnesses in favour of the anthropogenic origin of the signals.
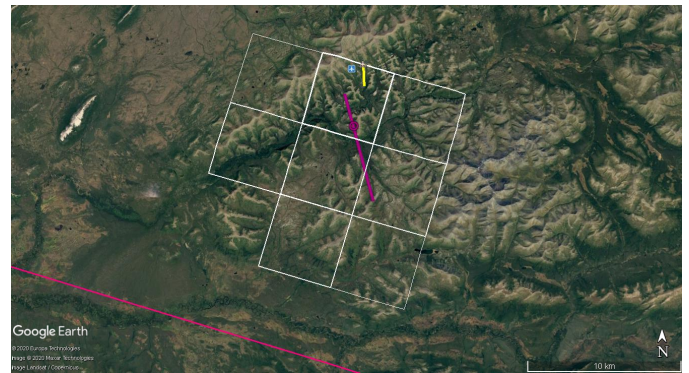

Fig. 7. Google Earth map for the TUS161031a event. The short yellow line corresponds to the runway of the Sparrevohn AFC Airport.

EAS-like events registered above oceans are more interesting as regards a possible astrophysical origin. In total, we found 15 such events, four of which had at least three active channels and were registered in good observational conditions. The geographical locations of the events are shown in Fig. 8.

One of these events was registered above the Pacific ocean, approximately 150 km West from Isla Guadelupe, three hours earlier than the event near the Sparrevohn airport. The light curve of six active channels of the event TUS161031b is shown in Figure 9. Due to big asymmetry, it has a rather long FWHM ($\sim 80\,\mu$s) and 3 times smaller amplitude than the TUS161031a event.
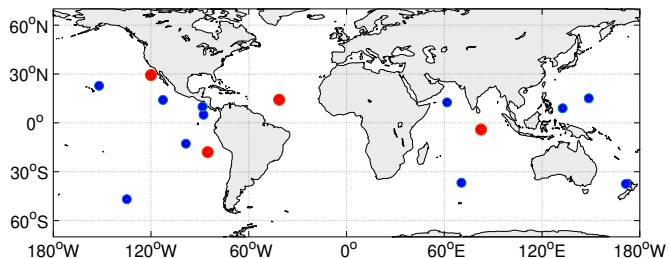
Fig. 8. Geographical locations of EAS-like events registered above oceans. Shown in red are four the most interesting ones, see the text for details.

However, the hit pixels form a compact group near the edge of the detector FoV, therefore, part of the signal may be missing. An analysis of the waveforms did not allow us to identify a noticeable displacement of the image. This means that the radiation source is either stationary (or moves with non-relativistic speeds), or the event is quasi-vertical (with a $\theta < 10°$).
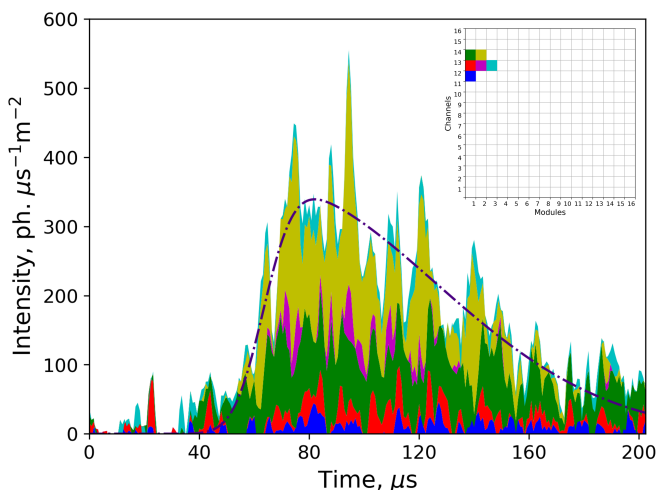

Fig. 9. Light curve of the TUS161031b event registered above the Pacific Ocean.

The TUS161031b event was registered in very good observational conditions. The Vaisala network (Said & Murphy, 2016) did not register a single lightning strike in around 1000 km from the event location within ±30 s from the trigger time stamp. The atmosphere around the place was close to an absolutely clear one. For example, the GOES-15 satellite map did not reveal any high-altitude clouds around the place and time of registration of TUS161031b.

Vessels are another possible origin of the signal. An analysis of the data available at the Global Fishing Watch Network (2021) did not reveal any fishing activity in the region around the night of registration. However, according to the Marine Traffic Density Maps (2021), the event was registered near an intensive marine route. We did not find any information about cargo or other types of ships in the FoV of TUS at the moment of the trigger but we cannot unequivocally exclude an artificial source of light as the origin of the event.

The situation with three other interesting events registered above oceans is similar to the one described above: they were recorded in good observational conditions but the low number of active channels does not allow us to reconstruct the arrival direction of the source of light accurately, and we did not find enough information about marine traffic to exclude an anthropogenic origin of the signals.

7. Transient atmospheric events: ELVEs and unusual far-from-thunderstorm flashes

A number of fast processes developing at time scales of a few hundred microseconds but different from EAS-like events were registered in the EAS mode of observations. Among them, there are 26 so called ELVEs, which are the type of transient luminous events (TLEs) that represent expanding luminous rings in the ionosphere at the height of 80–90 km. The duration of an ELVE is less than 1 ms and they can expand over 300 km laterally. It is believed that they are the result of ionospheric electrons heating by the upward electromagnetic impulse radiated by the lightning discharge current (Inan et al., 1997). According to the ISUAL global experimental data (Chen et al., 2008), ELVEs are the most common type of TLEs: around 50% of all TLEs were found to be ELVEs.

Usually, ordinary (single) ELVEs are caused by a cloud-to-ground lightning of any polarity. Several of the ELVEs registered by TUS have a more complicated space-time pattern: two or more rings were observed moving with a high speed across the field of view.

In (Marshall et al., 2015), simulations of double ELVEs were made and it was demonstrated that these ELVE doublets are the ionospheric signature of compact intra-cloud discharges (CIDs). CIDs are extremely powerful compact discharges that are thought to occur near the top of some thunderclouds. These discharges have duration of 20–30 μs. The phenomenon is known to be the source of a very intensive electromagnetic pulses (EMP).

One example of a double ELVE, measured by TUS on 10th April, 2017, at 13:06:59 UTC is presented in Fig. 10. On the pixel map two separate rings are clearly seen. These rings correspond to two peaks in the waveforms shown in the right part of figure (signals of two channels are given for comparison). The first ring is brighter. It corresponds to interaction of ionosphere with a direct electromagnetic wave from lightning. The second ring is caused by an electromagnetic emission of lightning which is reflected from ground. The delay Δt between two rings of the double ELVE is simply calculated from the geometry of measurements,

$$c\Delta t = \left[L^2 + (H + h_{\text{EMP}})^2\right]^{1/2} - \left[L^2 + (H - h_{\text{EMP}})^2\right]^{1/2},$$

where L is the distance between the pixel FoV center and the projection of the source position on the ground, H is an altitude of the ionospheric layer where ELVE is developed and h_{EMP} is the EMP source altitude.

If we measure Δt then we can determine h_{EMP} given H and L. The estimation of H is well known from numerous ELVEs observations. For example, Van der Velde & Montanyà (2016) demonstrated that an ELVE altitude during individual nights
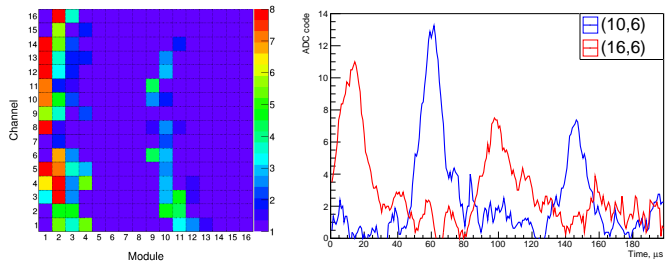
Fig. 10. A double ELVE measured by the TUS detector on 10th April, 2017. Left: pixel map, two bright rings are seen. Right: the waveforms of the two channels (10,6) and (16,6) (blue and red lines), each comprise two peaks with a time delay of ~85 μs.

ranges between 83 km and 93 km with the median of 87.1 km. The uncertainty of L is much bigger. Thunderstorms occupy a large area (more that 100 km in diameter), which means a large area of cloud coverage as well. In this case it is difficult to determine L accurately.

The ELVE shown in Fig. 10 was registered above the West coast of New Britain (coordinates of the TUS FoV center were 5.68°S, 148.40°E). To analyze thunderstorm activity at the time of registration, data from the ground-based lightning location network Vaisala GLD360 (Said & Murphy, 2016) were used. A thunderstorm with numerous lightning discharges was measured to the north of the detector FoV, which corresponds to the direction of the ELVE arrival.

A method based on probabilistic inference was developed and applied to the TUS data. For the ELVE registered on 10th April, 2017, we obtained $h_{EMP} \sim 25 \pm 7$ km. The accuracy of the method strongly depends on the number of channels used for the analysis. Besides this, the TUS data suffer from a number of dead pixels, weak channels and signal saturation. This complicates applying the method to the TUS data. However, it can be efficiently applied to data of missions such as Mini-EUSO or K-EUSO, which have an order of magnitude more pixels and a better spatial resolution.

While it is rather straightforward to identify ELVEs in the data due to the specific pattern of the signal, the nature of some other bright moving flashes registered in the EAS mode is puzzling. Let us consider two examples of such events. The first of them was registered on 5th September, 2016, near Sardinia. The signal was so strong that it immediately saturated a number of channels and showed a complicated dynamics afterwards. The waveforms of some active channels are shown in Fig. 11.

At the moment TUS160905 was observed, the sky was clear, and no lightning strikes were registered by the Vaisala network within 1000 km from the event. The cloud form and cover showed in Fig. 12 depict clear sky at the event position, see also Fig. 6. Thus, there are no obvious reasons for an atmospheric origin of the event. No possible sources of artificial light were found in the FoV of TUS. This makes the origin of the TUS160905 event an open question.

Another event that poses a similar puzzle was registered on 26th April, 2017, 150 km West from Australia. Fig. 13 presents waveforms of active channels of the event. Similar
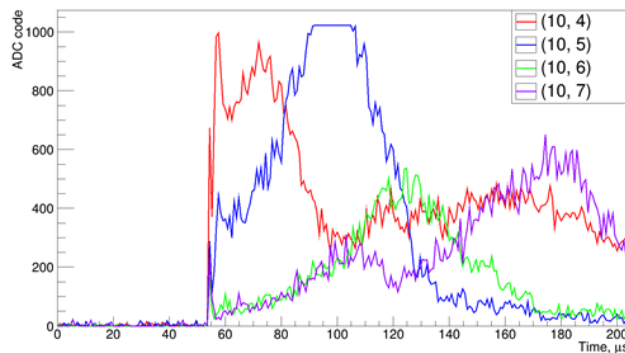

Fig. 11. Waveforms of the four active channels indicated in the inset for the TUS160905 event.
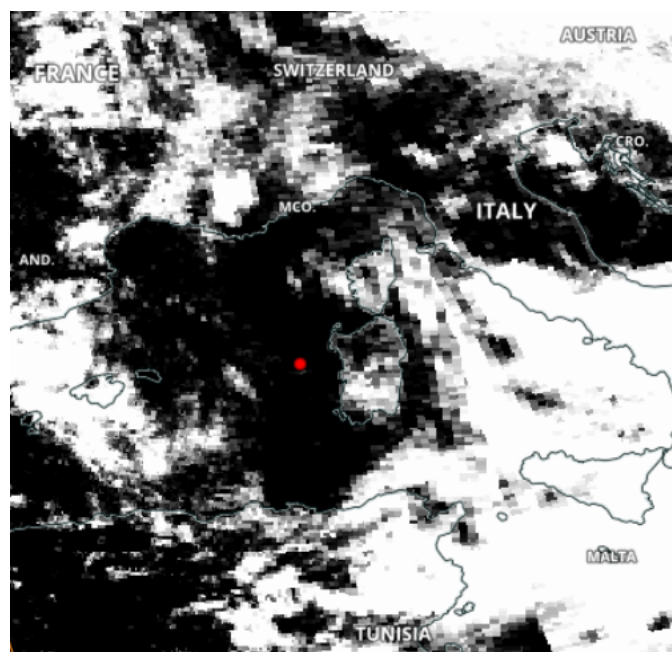

Fig. 12. Cloud cover from the MODIS Terra satellite at 2200 UTC, white parts indicate cloud cover, black parts indicate clear sky. The red dot indicates the position of the TUS160905 event.

to the TUS160905 event, an instantaneous growth of the signal was observed in a number of channels, and a complicated dynamics of the signal was found next. The atmosphere was clear, and the nearest thunderstorm took place in approximately 500 km from the TUS FoV (see Fig. 14). The first peak was so bright that it led to a channel saturation from the time of triggering until the end of the waveform. During the second part of the event, the peak of the signal moved along the photodetector modules with a relativistic speed. This allows one to estimate the zenith angle of the direction of the signal motion, which turned out to be close to horizontal ($\theta > 80°$). An explanation of the nature of the event does not currently exist.

A number of other bright flashes with different behaviour of the signal were registered in clear atmospheric conditions far from thunderstorm regions. Their origin is still unclear. Results
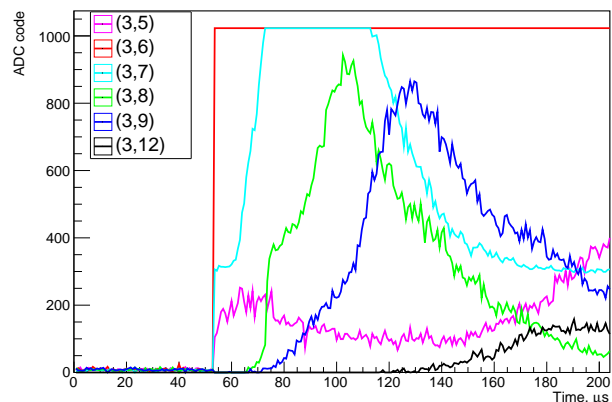
Fig. 13. Waveforms of active channels in the 3rd module in the TUS170426 event.
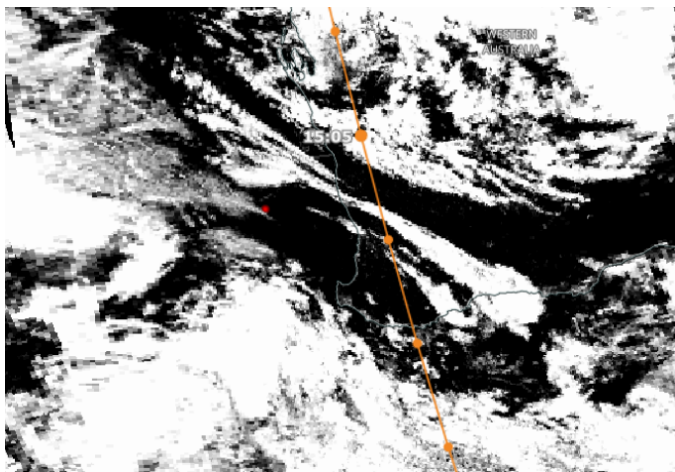

Fig. 14. Cloud cover from the MODIS Terra satellite at 1509 UTC, white parts indicate cloud cover, black parts indicate clear sky, while the orange line is the orbit track with times of acquisition. The red dot indicates the position of TUS170426 event.

of their analysis will be reported elsewhere.

8. Meteors

It was shown by (Khrenov & Stulov, 2006) that the fluorescence light produced by meteors with velocities ∼ 30 km/s can be registered by the TUS detector in the slowest mode of observations with time sampling 6.55 ms and duration of the record ≈ 1.7 s. During 250 h of nighttime observations in this "meteor" mode, the TUS detector measured at least 13 events with a typical meteor signal profile. Some of them were discussed in (Klimov et al., 2019). These events were distributed around the globe, four of them over the land and the rest over the sea.

The typical behaviour of the integrated light curve of the TUS meteor events with a monotonically increasing signal and a rapid decay is presented in Fig. 15. Some of the events had one, two or even more intermediate peaks, probably due to low sensitivity pixels. In several cases, the characteristic rise and

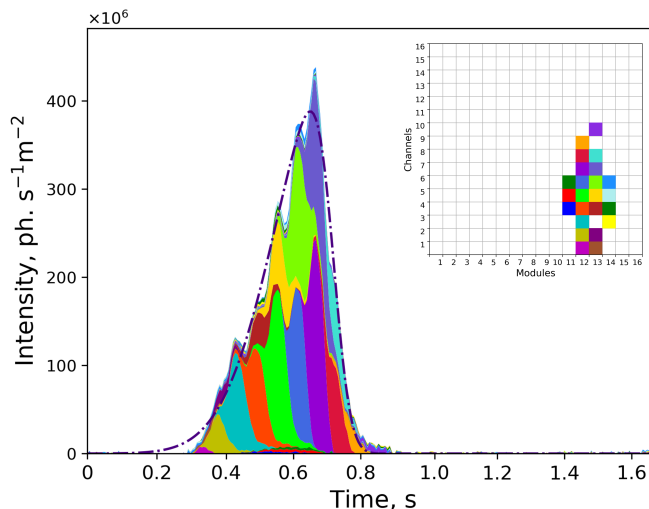decay times of the signal were close to each other, and the light curve looked almost symmetric.

Fig. 15. Light curve of the meteor event TUS170318b and its Skew Gaussian approximation. Inset: pixel map with hit pixels.

The reconstruction of these events assumes the presence of some a priori information about the speed of the meteor. The reconstructed arrival direction of several of the TUS meteor events coincided within the error with the radiant of a meteor shower that existed at the time of registration. On the other hand, some events were recorded at a time when it was not possible to observe a meteor shower in a given geographical location (shower radiant was below the horizon), indicating, a sporadic origin of these meteors.

All registered meteors have a fairly high brightness because the trigger parameters were optimized for fast EAS events. The absolute magnitude M_U (in terms of observation at 100 km altitude at the observer's zenith) in U-band ranges from -3.7 to +2.6 with the threshold estimated as $M_{U,thr} \approx 2.6$ for most sensitive channels and $M_{U,thr} \approx 2.1$ for most of the detector's FoV. The corresponding thresholds in V-band are 2.9 and 2.4. In particular, the TUS170318b meteor shown in Fig. 15 had $M_U \approx 0.6$ at maximum. One of the recorded meteors, TUS170321, was very bright, with $M_U \approx -3.7$. Its image occupied a significant part of the detector FOV, and its duration exceeded 1.3 s.

9. Nuclearites

Macroscopic dark matter, generally called macros (Jacobs et al., 2015), is a broad class of dark-matter candidates, that represents an alternative to conventional particle dark matter. The theoretical motivation to believe that a large fraction of the mass and baryon number of the early Universe has survived in the form of nuggets of strange quark matter, composed of approximately the same number of up, down and strange quarks, was provided by the work of (Witten, 1984). Their mass can range from ordinary nuclei to macroscopic objects, up to neutron stars. According to (De Rujula & Glashow, 1984), nuclearites are strange quark nuggets, with overall neutrality en-

sured by an electron cloud that surrounds the nuclearite core, forming a sort of atom. Nuclearites travelling with galactic velocities are protected by their surrounding electrons against direct interactions with the atoms they might hit. Therefore, they only lose energy in elastic collisions with atoms in the medium. A fraction of the energy is converted to the black-body radiation from an expanding cylindrical thermal shock wave. It was argued by (De Rujula & Glashow, 1984) that nuclearites having mass $m > 10^{-14}$ g penetrate the atmosphere, while those with $m > 0.1$ g can pass freely though an Earth diameter. The dark matter density near the Sun ρ_{DM} is of the order of 0.35 GeV cm^{-3} (Kafle et al., 2014). This gives a limit on an isotropic flux of the nuclearites at a velocity v in the observer's frame to be $\rho_{DM}v/(4\pi mc^2)$.

Nuclearites and similar particles, as for example neutral Q-balls (Kusenko et al., 1998), have been searched for using different approaches (Astone et al., 1993; Shirk & Price, 1978; Orito et al., 1991; Cecchini et al., 2008; Nakamura et al., 1991; Ambrosio et al., 2000; Bouta et al., 2021; Piotrowski et al., 2020; Price, 1988). The experiments can be characterized by the detection area and by the minimum nuclearite mass that can be detected, usually computed for a speed of 250 km/s. It is important to have different techniques to search for such exotic particles due to the uncertainties in the energy losses. The possibility to employ fluorescence detectors to search for unusual particles in the primary flux such as quark matter and weakly interacting particles produced in the interactions of the cosmic-ray flux with the atmosphere was first performed by the Fly's Eye Collaboration (Baltrusaitis et al., 1985). A search for nuclearites with a space-based observatory was later on proposed by the JEM-EUSO collaboration (Adams Jr. et al., 2015b). A general discussion on the search for macroscopic dark matter with fluorescent detectors is reported in (Sidhu Singh et al., 2019), where a formalism different from (De Rujula & Glashow, 1984) was introduced. More recently, it was pointed out by Anchordoqui et al. (2021) that for a reference mass of 1 g, there is a discrepancy in the macro luminosity of about 14 orders of magnitude between the predictions of the two formalisms described by De Rujula & Glashow (1984) and by Sidhu Singh et al. (2019). However, none of the two can be ruled out. In the following, we present a preliminary estimate of the TUS limits assuming (De Rujula & Glashow, 1984). This analysis has to be considered as a methodological study in view of future space-based detectors, and the presented results as preliminary. In fact, TUS was not developed with such an objective, therefore, the performance is not indicative of the full potential of a space-based telescope. However, it can provide a guidance and confirm the feasibility of the technique. The sensitivity is obtained under general assumptions that, despite having a rationale behind it, still needs to be carefully verified. This will be the subject of a future publication. A detailed description of the analysis on the search for nuclearites and on the estimation of the geometrical aperture is reported in (Shinozaki et al., 2019).

The principle of the nuclearite search by TUS is based on the detection of a moving light spot in the atmosphere. The radiation mechanism of the nuclearites in the atmosphere and ob-

servable characteristics of such spots were modeled in (De Rujula & Glashow, 1984) for an assumed nuclearite velocity of 250 km/s considered as a typical velocity of the Galaxy near the Sun. A small modification is applied here to their formula to allow for arbitrary velocities. The apparent brightness of the nuclearite expressed in stellar magnitude units $\mathcal{M}$ follows the relation:

$$\mathcal{M} = 10.8 - 1.67 \log_{10}(m/1\,\mu g) + 5 \log_{10}(r/10\,\text{km}) \\ - 7.5 \log_{10}(v/250\,\text{km s}^{-1}), \quad (1)$$

where r is the distance to the observer. For simplicity, we also assume that the flux, defined for the V-band magnitude ($\lambda = 550$ nm) is constant over the wavelength range of TUS (250–400 nm). According to (De Rujula & Glashow, 1984), the maximum height where a nuclearite at $v = 250$ km/s can effectively generate the light, assuming a constant atmospheric scale height, is:

$$h_{max} = 2.7\,\text{km} \cdot \ln(m/1.2 \cdot 10^{-5}\,\text{g}). \quad (2)$$

We used a realistic density profile function to convert the corresponding air density ρ into height, which lowers h_{max}.

To search for nuclearites, TUS data acquired in the "meteor" mode were selected by requiring a nocturnal background level according to the high voltage level, the sub-satellite point at sea level at least 75 km away from the coast to minimize the effect of anthropogenic lights and the zenith angle of the Moon above 90° to eliminate direct moonlight on the focal surface of the detector. Moreover, only the good-quality PMTs, whose gain was estimated in flight to be of the order of 10^6, were considered.

In TUS, the main observable are the light curve and the angular velocity ω. In case of meteors, the light curve can drastically change in time due to ablation processes and fragmentation of the meteoroid, giving birth to even more than one peak. On the other hand, the intensity of the light spot from a nuclearite is expected to change only monotonously with distance r. TUS can only measure the perpendicular component $v_\perp$ seen from the observer, which is given by $r\omega$. The speed of the Sun relatively to that of the Galactic Center is usually considered to define the relative velocity of the nuclearites. However, by considering also the escape velocity from the Galaxy, an upper bound is set to the "relative" velocity in the frame of the observer at ~800 km/s. For this reason the estimation of $\mathcal{M}$ takes into account also the velocity as a parameter. The definition of the aperture is done for three different cases: a) the standard one of 250 km/s, b) a lower bound at 75 km/s to be just above the limit of the meteor speed, c) 800 km/s as an upper limit.

Since nuclearites may be seen as "fast" moving events, we looked for events in which the fastest peak channel was shifting faster than 0.13 rad/s, i.e. $v_\perp \geq 60$ km/s. After this selection, only 76 events remained, and on these we applied a visual inspection. None of the above candidates had a moving light spot compatible with simulations of nuclearite light tracks.

To interpret the data and to estimate the performance of the instrument, we carried out a full simulation study including radiation processes in atmosphere and detector response. To emulate the observation conditions, we checked the selection criteria along the orbit every 5 s by calculating the distance to the

coast and Moon's zenith angle. To estimate the "on-time" T_0, we assumed that TUS was active for data taking in any 5-s segments if the elapsed time after the last trigger was longer than 53 s. The first event after TUS entered the Earth's umbra was excluded. By summing up these active segments, T_0 is estimated to be 47.4 hours. To include the presence of clouds that might reduce the observation area, we employed the MERRA2 dataset. It provides the global weather parameters outputs on 0.5°(latitude) × 0.625°(longitude)-grid points. The cloud-top height map is renewed every hour and the value is picked up every 5 s below the TUS position. To generate a simulated event from a nuclearite, we randomly sampled the conditions from all the active times to refer the cloud-top height to the TUS height and position. For an input mass of nuclearite m, the arrival direction and impact points are uniformly distributed onto a sphere with a radius R_0 beneath TUS. Among the generated N_{sim} events, the number of the events N_{sel} that pass the event selection allows to compute the aperture as

$$A_0 = 2\pi^2 R_0^2 \cdot (N_{sel}/N_{sim}).$$

The atmospheric model includes air and ozone densities (Kneizis et al., 1996) to take into account wavelength-dependent Rayleigh scattering and ozone absorption. As a result, the maximum height of light emission by nuclearites is modified, from Eq. (2) and it is in general lower. Therefore, the effective volume of light emission in atmosphere decreases. As an example, at 1 kg mass it becomes ~ 35 km to be compared with ~ 50 km from the original formula. We generated the light from nuclearites only in the volume of atmosphere between the cloud-top-height and h_{max}. We applied the ray trace and electronics response simulations with the background level and its fluctuation based on real data taken from the last TUS event at the sampled time. For all channels and ticks, the background is added with a Gaussian random generation. Simulation of nuclearite events was performed. To discriminate them from meteors and other moving events, it is important to have many channels with significant signals in order to determine the angular velocity and light curve properly. To estimate a sensitivity in terms of "aperture" of such an analysis, we applied relatively tight cuts on the simulated events. In addition to previous conditions, we required further stringent cuts such as $\geq$ 10 channels with the maximum counts above 25σ and $\geq$ 10 ticks (~ 66 ms) available to compute the motion analysis. Combinations of $m = 0.1$, 1 and 100 kg, and $v = 75$, 250, and 800 km/s were simulated.

To translate the geometrical aperture into an exposure, an estimation of the on-time T_0 and of the limiting magnitude $\mathcal{M}$ is needed. These two numbers are not straightforward. In particular, the 53–60 s off-time of the detector between events does not allow having an exact knowledge of the illumination conditions between two consecutive triggers, which prevents a precise assessment of the limiting magnitude $\mathcal{M}$ at each instant. Moreover, a calibration of the instrument is still in progress. Therefore, we present the TUS sensitivity under two assumptions that still require further investigation. In the current estimate, we assume the capability of detecting masses above 100 g which corresponds to $\mathcal{M} < +6$ according to Eq. (1), which is compliant with the limits in meteor brightness (note the relation of the

brightness used here and in Section 8: $\mathcal{M} = M_V + 3.5$.). Moreover, we assume $T_0 \sim 2$ day on-time, which implies that the detector was always functioning between consecutive triggers with weather conditions allowing the detection of nuclearites with the above limiting magnitude. Under these assumptions, our preliminary limits at 90% confidence level are reported in Fig. 16 and compared with other experiments. The intersection of the lines at different light speed takes into account opposite aspects that act conversely in terms of chance of detecting the nuclearites. In fact, according to Eq. 1 fast objects are more luminous but their residence time in the pixel FoV is shorter and vice versa for slow events.
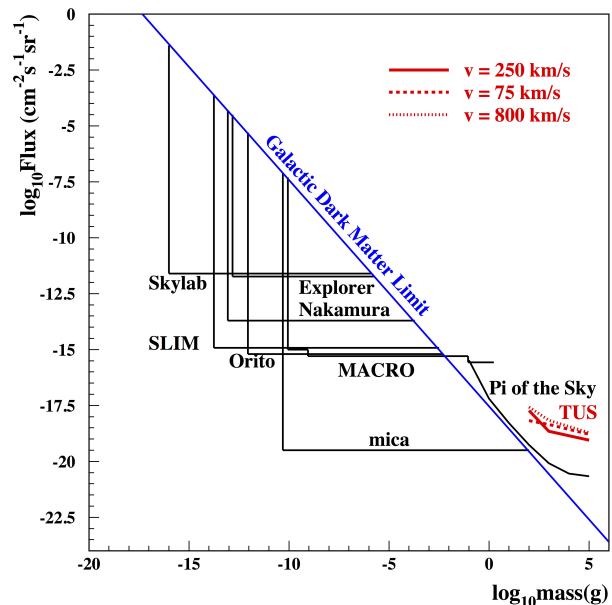

Fig. 16. Preliminary limits on nuclearite sensitivity of TUS compared with previous experiments taken from (Astone et al., 1993; Cecchini et al., 2008; Ambrosio et al., 2000; Piotrowski et al., 2020; Price, 1988) under the assumptions outlined in the text.

Despite the fact that the TUS limits are on the right of the Galactic dark matter limit line, the plot shows the potential of a space-based detector to provide comparable flux limits to other experiments, thanks to the large aperture. We underline that most of the limitations on the present result come from the fact that the instrument was not designed for this search, it was operated in "meteor" mode for only a short time, and an accident occurred at the beginning of the mission. Despite those limits and constraints, the result supports the findings by (Anchordoqui et al., 2021; Abdellaoui et al., 2017), which indicate that Mini-EUSO and POEMMA have the opportunity to cross the dark matter limit line providing estimations in an interesting phase space.

10. Auroral lights

One of the unexpected results of the TUS mission was the discovery of fast near-UV pulsations in the region of the auroral

oval. The Lomonosov satellite had a polar sun-synchronous orbit with an inclination of 97.3°, which provided measurements up to the high latitudes on the night side of the orbit. Thus the detector FoV used to cross the region of aurora lights and it was possible to study fine temporal and spatial structure of the aurora oval with high sensitivity. In the meteor mode, about 2500 events were measured with latitudes > 50° in Northern hemisphere. Among them, 66 events with an interesting temporal structure were selected. These signals differ from clouds, cities and other well-known sources of light in the atmosphere and occur above land and ocean.

The observed signals have a very diverse structure with characteristic frequencies of the order of 1–10 Hz. The most frequently recorded pulsations lie in the region from 3 Hz to 5 Hz but there are events with a frequency of up to 20 Hz. One example of waveform is shown in Fig. 17. The luminescence regions are localized spatially with a characteristic size about 10 km. Several different pulsation regions with different temporal structures (waveforms) could be observed simultaneously in FoV of the telescope.
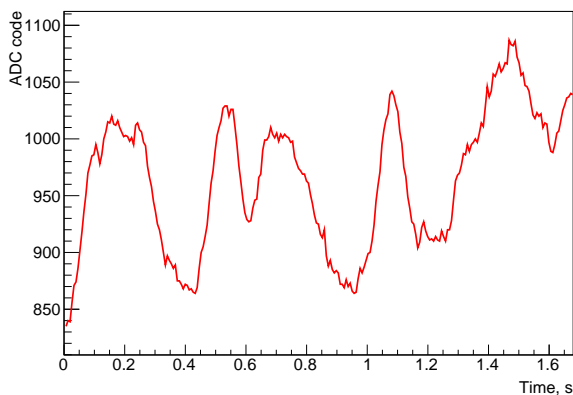

Fig. 17. Waveform of one pixel (No.219) of the event measured on 6th January, 2017, at 05:18:26 UTC.

An analysis of the geographical distribution and geomagnetic conditions indicates that the events were measured at the equatorial border of the aurora zone. Geographical distribution of UV pulsating events is shown in Fig. 18. Aurora oval is also well seen on the active time map (fig. 4). Pulsating events locations obviously repeat shape of the oval.

Their location does not depend on geomagnetic activity level which is typical for the other aurora-zone events. The maximum portion of the pulsations is recorded in the L-shells range from 4 to 6. The frequency of events' occurrence correlates with geomagnetic activity.

The spatio-temporal structure of the events is similar to flickering auroras observed earlier (Sakanoi et al., 2005) and internal modulations of pulsating auroras related to a high-energy part of precipitating electrons caused by lower-band chorus waves (Miyoshi et al., 2020). However, their nature and the occurrence mechanism of is not yet clear. Further research based on high-sensitive orbital observations is required to obtain detailed characteristics of this type of signals.
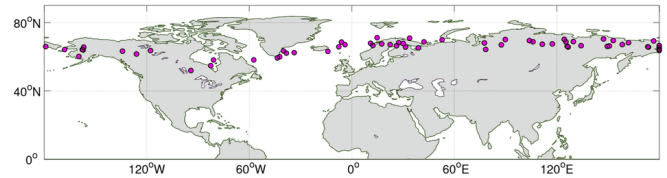

Fig. 18. Map of selected events with near-UV pulsations in the auroral zone.

11. Conclusions

The TUS detector was the first space-based mission designed for ultra-high energy cosmic ray measurements. Its active operation lasted from 19 May 2016 till 30 November 2017. During the mission, several acquisition modes with different temporal resolution were tested to sense various physical phenomena, with the total geometrical exposure in the EAS mode reaching approximately 1550 km^2 sr yr. A number of EAS-like events that have a typical light curve and demonstrate a movement in the FoV at a relativistic velocity were registered. The vast majority of these events were recorded over land, which witnesses in favour of their anthropogenic origin. For five of them, there is a correlation between their arrival directions and airport runways. A number of events with EAS-like light curves were recorded above oceans, which reduces the likelihood of their anthropogenic origin. However, the number of triggered pixels of the photodetector was small for these events, which makes it difficult to determine a directional movement. This is due to the insufficient spatial resolution of TUS, which will be an order of magnitude better in the future projects (K-EUSO and POEMMA), and will allow us to study such events in more detail.

A new version of the ESAF software framework that includes the TUS detector was developed to understand the origin of EAS-like events and to estimate the sensitivity of TUS to UHECRs. The energy evaluation for some of them with ESAF (for example, the TUS161003 event) provides a value of one order of magnitude higher than could be expected from UHECRs. This can be interpreted in several ways. The most probable is the anthropogenic origin as was mentioned above. However, an astrophysical hypothesis associated with relativistic dust grains is also considered.

The TUS detector registered various UV phenomena which constitute the background for UHECR measurements. Among them are anthropogenic lights, thunderstorm activity and lightning discharges, upper atmosphere transient luminous events, polar lights, meteors and other phenomena, providing in some cases an imaging of these signals with an unprecedented sensitivity and time resolution. The capability of observing meteors allowed us to perform a methodological study and search for macroscopic dark matter events. The geometrical aperture of TUS for nuclearites and the sensitivity of the device to such studies were estimated. The importance of associating all the above observations with an assessment of the weather conditions was studied and the methodology was presented and applied to specific events.

The analysis of the TUS data is still ongoing. Recently, we

applied two different types of neural networks to classify the TUS data obtained in the EAS mode of observations (Zotov & Sokolinskiy, 2020; Zotov, 2021). This allowed us to find a large number of weak signals that were not noticed when applying conventional techniques.

Generally, we believe the TUS experiment has demonstrated that the orbital fluorescent technique has a strong potential to measure and recognize a relativistic motion in the UV range in the atmosphere, to reconstruct the direction and energy of different events, to study phenomena that avoid registration from the ground. On the other hand, the experience of the TUS mission reveals the difficulties of a space-based experiment that needs an accurate monitoring of the rapidly changing background illumination and a high-quality control of the sensitivity of the equipment. The TUS detector demonstrated a multi-functionality of an orbital fluorescent observatory and its usefulness for various astrophysical and geophysical studies. It provides an invaluable experience for the implementation of the future orbital missions like K-EUSO and POEMMA. The methods developed for the TUS data analysis and its results are actively employed for studying and interpreting data of the Mini-EUSO telescope, which is currently operating at the International Space Station.

References

Aab, A., Abreu, P., Aglietta, M. et al. (2020). Measurement of the cosmic-ray energy spectrum above 2.5×10^{18} eV using the Pierre Auger Observatory. *Physical Review D*, *102*, 062005.

Abdellaoui, G., Abe, S., Acheli, A. et al. (2017). Meteor studies in the framework of the JEM-EUSO program. *Planetary and Space Science*, *143*, 245–255.

Abdellaoui, G., Abe, S., Adams Jr., J. et al. (2018). EUSO-TA – first results from a ground-based EUSO telescope. *Astroparticle Physics*, *102*, 98–111.

Adams Jr., J., Ahmad, S., Albert, J.-N. et al. (2013). An evaluation of the exposure in nadir observation of the JEM-EUSO mission. *Astroparticle Physics*, *44*, 76–90.

Adams Jr., J., Ahmad, S., Albert, J.-N. et al. (2015a). The EUSO-Balloon pathfinder. *Exper. Astronomy*, *40*, 281–299.

Adams Jr., J., Ahmad, S., Albert, J.-N. et al. (2015b). JEM-EUSO: Meteor and nuclearite observations. *Exper. Astronomy*, *40*, 253–279.

Adams Jr., J., Ahmad, S., Albert, J.-N. et al. (2015c). The JEM-EUSO mission: An introduction. *Exper. Astronomy*, *40*, 3–17.

Adams Jr., J., Anchordoqui, L., Apple, J. et al. (2017). White paper on EUSO-SPB2. arXiv:1703.04513.

Ambrosio, M., Antolini, R., Aramo, C. et al. (2000). Nuclearite search with the MACRO detector at Gran Sasso. *Eur. Phys. J. C*, *13*, 453–458.

Anchordoqui, L. A., Bertaina, M. E., Casolino, M. et al. (2021). Prospects for macroscopic dark matter detection at space-based and suborbital experiments. *EPL Journal*, *135*, 51001.

Anzalone, A., Bertaina, M., Briz, S. et al. (2019). Methods to retrieve the cloud-top height in the frame of the JEM-EUSO mission. *IEEE transactions on geoscience and remote sensing*, *57*, 304.

Astone, P., Bassan, M., Bonifazi, P. et al. (1993). Upper limit for nuclearite flux from the Rome gravitational wave resonant detectors. *Phys. Rev. D.*, *47*, 4770–4773.

Bacholle, S., Barrillon, P., Battisti, M. et al. (2021). Mini-EUSO mission to study Earth UV emissions on board the ISS. *Astrophys. J. Suppl. Series*, *253*(2).

Baltrusaitis, R., Cassiday, G., Elbert, J. et al. (1985). Limits on deeply penetrating particles in the > 10^{17} ev cosmic-ray flux. *Phys. Rev. D*, *31*, 2192–2198.

Benson, R., & Linsley, J. (1981). Satellite observation of cosmic ray air showers. In *Proc. 17th Int. Cosmic Ray Conf.* (pp. 145–148). volume 8.

Berat, C., Bottai, S., De Marco, D. et al. (2010). Full simulation of space-based extensive air showers detectors with ESAF. *Astroparticle Physics*, *33*(4), 221–247.

Bertaina, M. (2021). An overview of the JEM-EUSO program and results. In *Proc. 37th Int. Cosmic Ray Conf.* PoS(ICRC2021)406.

Bonavita, M., Hólm, E., Isaksen, L., & Fisher, M. (2015). The evolution of the ECMWF hybrid data assimilation system. *Quarterly Journal of the Royal Meteorological Society*, *142*(694), 287 – 303.

Bouta, M., Moussa, A., Tayalati, Y. et al. (2021). Nuclearite search with ANTARES. arXiv:2107.13479.

Casolino, M., Bertaina, M., Belov, A. et al. (2017). KLYPVE-EUSO: Science and UHECR observational capabilities. In *Proc. 35th Int. Cosmic Ray Conf.* PoS(ICRC2017)368.

Cecchini, S., Cozzi, S., Di Ferdinando, D. et al. (2008). Results of the search for strange quark matter and Q-balls with the SLIM experiment. *Eur. Phys. J. C*, *57*, 525–533.

Chen, A. B., Kuo, C.-L., Lee, Y.-J. et al. (2008). Global distributions and occurrence rates of transient luminous events. *Journal of Geophysical Research: Space Physics*, *113*(A8), n/a–n/a. doi:10.1029/2008JA013101. A08306.

De Rujula, A., & Glashow, S. (1984). Nuclearites—a novel form of cosmic radiation. *Nature*, *312*, 734–737.

d'Entremont, R., & Thomason, L. (1987). Interpreting meteorological satellite images using a color-composite technique. *Bulletin of the American Meteorological Society*, *68*(7), 762 – 768.

Fenu, F., Shinozaki, K., Zotov, M. et al. (2021). Estimation of the exposure of the TUS space-based observatory. In *Proc. 37th Int. Cosmic Ray Conf.* PoS(ICRC2021)333.

Global Fishing Watch Network (2021). `https://globalfishingwatch.org/`.

Heck, D., Knapp, J., Capdevielle, J. et al. (1990). Corsika: A Monte-Carlo code to simulate EAS. `http://www-ik.fzk.de/corsika/`.

Ilina, N., Kalmykov, N., & Prosin, V. (1992). Cherenkov radiation and parameters of extensive air showers. *Sov. J. Nucl. Phys.*, *55*, 1540–1547.

Inan, U. S., Barrington-Leigh, C., Hansen, S. et al. (1997). Rapid lateral expansion of optical luminosity in lightning-induced ionospheric flashes referred to as "elves". *Geophysical Research Letters*, *24*, 583–586. doi:10.1029/97GL00404.

Jacobs, D., Starkman, G., & Lynn, B. (2015). Macro dark matter. *Mon. Not. Roy. Astron. Soc.*, *450*(4), 3418–3430.

Japanese Coast Guard (2021). `https://www1.kaiho.mlit.go.jp/KOHO/syoshi/furoku/na16-data.pdf`, `https://www1.kaiho.mlit.go.jp/KOHO/syoshi/furoku/na16-rei.pdf`.

Kafle, P., Sharma, S., Lewis, G., & Bland-Hawthorn, J. (2014). On the shoulders of giants: properties of the stellar halo and the Milky Way mass distribution. *The astrophysical J.*, *794*, 59.

Khrenov, B., Garipov, G., Kaznacheeva, M. et al. (2020). An extensive-air-shower-like event registered with the TUS orbital detector. *Journal of Cosmology and Astroparticle Physics*, *3*, 033.

Khrenov, B., Kalmykov, N., Klimov, P., Sharakin, S., & Zotov, M. (2021). Relativistic dust grains: a new subject of research with orbital fluorescence detectors. In *Proceedings of 37th International Cosmic Ray Conference* Pos(ICRC2021)315.

Khrenov, B., Panasyuk, M., Alexandrov, V. et al. (2001). Space program KOSMOTEPETL (project KLYPVE and TUS) for the study of extremely high energy cosmic rays. *AIP Conference Proceedings*, *566*, 57.

Khrenov, B. A., Klimov, P. A., Panasyuk, M. I. et al. (2017). First results from the TUS orbital detector in the extensive air shower mode. *Journal of Cosmology and Astroparticle Physics*, *9*, 006. arXiv:1704.07704.

Khrenov, B. A., & Stulov, V. P. (2006). Detection of meteors and sub-relativistic dust grains by the fluorescence detectors of ultra high energy cosmic rays. *Advances in Space Research*, *37*(10), 1868–1875.

Klimov, P., Khrenov, B., Kaznacheeva, M. et al. (2019). Remote sensing of the atmosphere by the ultraviolet detector TUS onboard the Lomonosov satellite. *Remote Sensing*, *11*(20).

Klimov, P., Panasyuk, M., Khrenov, B. et al. (2017). The TUS detector of extreme energy cosmic rays on board the Lomonosov satellite. *Space Science Reviews*, *8*, 1687–1703.

Kneizis, F., Abreu, L., Anderson, G. et al. (1996). The MODTRAN 2/3 Report and LOWTRAN 7 Model.

Kotera, K., & Olinto, A. (2011). The astrophysics of ultrahigh energy cosmic rays. *Ann.Rev.Astron.Astrophys.*, *49*, 119–153.

Kusenko, A., Kuzmin, V., Shaposhnikov, M., & Tinyakov, P. (1998). Experimental signatures of supersymmetric dark-matter Q-balls. *Phys. Rev. Lett.*, *80*, 3185–3188.

Marine Traffic Density Maps (2021). https://www.marinetraffic.com.

Marshall, R. A., Silva, C. L., & Pasko, V. P. (2015). Elve doublets and compact intracloud discharges. *Geophysical Research Letters*, *42*(14), 6112–6119.

MERRA data (2021). https://gmao.gsfc.nasa.gov/reanalysis/MERRA-2/.

Miyoshi, Y., Saito, S., Kurita, S. et al. (2020). Relativistic electron microbursts as high-energy tail of pulsating aurora electrons. *Geophysical Research Letters*, *47*(21), e90360.

Nagano, M., Kobayakawa, K., Sakaki, N., & Ando, K. (2004). New measurement on photon yields from air and the application to the energy estimation of primary cosmic rays. *Astrop. Phys.*, *22*, 235–248.

Nakamura, S., Orito, S., Suzuki, T. et al. (1991). A new limit on the flux of strange matter. *Phys. Lett. B*, *263*(3-4), 529–533.

Olinto, A., Krizmanic, J., Adams Jr., J. et al. (2021). The POEMMA (Probe of Extreme Multi-Messenger Astrophysics) observatory. *J. of Cosmology and Astrop. Physics*, *6*, 007.

Orito, S., Imori, M., Yamamoto, K. et al. (1991). Search for supermassive relics with a 2000 m^2 array of plastic track detectors. *Phys. Rev. Lett.*, *66*, 1951–1954.

Parmar, A., Clavel, J., Catalano, O., & Santangelo, A. (2013). The Extreme Universe Space Observatory (EUSO) mission in the context of ESA. In *In Proc. 28th Int. Cosmic Ray Conf.* (pp. 1073–1076).

Pierog, T., Alekseeva, M., Bergmann, T. et al. (2004). First results of fast one–dimensional hybrid simulation of EAS using CONEX. arXiv:astro–ph/0411260v1.

Piotrowski, L., Malek, K., Mankiewicz, L. et al. (2020). Limits on the flux of nuclearites and other heavy compact objects from the Pi of the Sky project. *Phys. Rev. Lett.*, *125*, 091101.

Price, P. (1988). Limits on contribution of cosmic nuclearites to galactic dark matter. *Phys. Rev. D*, *38*, 3813–3814.

Rodell, M., Houser, P. R., Jambor, U. et al. (2004). The global land data assimilation system. *Bulletin of the American Meteorological Society*, *85*(3), 381 – 394.

Said, R., & Murphy, M. (2016). GLD360 upgrade: Performance analysis and applications. In *24th Int. Lightning Detection Conf. and Sixth Int. Lightning Meteorology Conf.* (p. 8pp).

Sakanoi, K., Fukunishi, H., & Kasahara, Y. (2005). A possible generation mechanism of temporal and spatial structures of flickering aurora. *Journal of Geophysical Research*, *110*, A03206.

Sharakin, S., & Ruiz Hernandez, O. I. (2021). Kinematics reconstruction of the eas-like events registered by the tus detector. *Journal of Instrumentation*, *16*(07), T07013.

Shinozaki, K., Montanaro, A., Bertaina, M. et al. (2019). Search for nuclearites by the satellite-based TUS air fluorescence detector. In *Proc. 36th Int. Cosmic Ray Conf.* PoS(ICRC2019)545.

Shirk, E., & Price, P. (1978). Charge and energy spectra of cosmic rays with $z \gtrsim 60$: the Skylab experiment. *The Astrophys. J.*, *220*, 719–733.

Sidhu Singh, J., Abraham, S., Covault, C., & G., S. (2019). Macro detection using fluorescence detectors. *J. of Cosmology and Astrop. Physics*, *1902*, 037.

Stecker, F., Krizmanic, J., Barbier, L. et al. (2004). Observing the ultrahigh-energy universe with OWL eyes. *Nucl. Phys. Proc. Suppl.*, *136C*, 433.

Tkachev, L., Grinyuk., A., Lavrova, M. et al. (2015). The TUS orbital detector simulation. In *Proc. 34th Int. Cosmic Ray Conf.* PoS(ICRC2015)610.

Van der Velde, O. A., & Montanyà, J. (2016). Statistics and variability of the altitude of elves. *Geophysical Research Letters*, *43*(10), 5467–5474.

Wiencke, L., & Olinto, A. (2017). EUSO-SPB1 mission and science. In *Proc. 35th Int. Cosmic Ray Conf.* PoS(ICRC2017)1097.

Witten, E. (1984). Cosmic separation of phases. *Phys. Rev. D*, *30*, 272–285.

Zotov, M. (2021). Application of neural networks to classification of data of the TUS orbital telescope. *Universe*, *7*(7).

Zotov, M. Y., & Sokolinskiy, D. B. (2020). The first application of neural networks to the analysis of the TUS orbital detector data. *Moscow University Physics Bulletin*, *75*(6), 657–664.